Seismic fragility curves for un-reinforced masonry walls

Elisa Lumantarna[1], Jerry Vaculik[2], Mike Griffith[2], Nelson Lam[1] and John Wilson[3]

[1] The University of Melbourne
[2] University of Adelaide
[3] Swinburne University of Technology

Abstract

Quasi-static experiments have been carried out on unreinforced masonry (URM) wall specimens subject to two-way bending and a range of boundary conditions. The hysteretic behaviour so obtained from the experiments have been used to generate fragility curves which define the probability of the wall sustaining minor to severe damage in an earthquake based on different levels of ground motion intensity and boundary conditions of the wall. The calculation for the fragility curves involves the generation of filtered accelerograms which take into account a range of earthquake scenarios, site conditions and building types. The generated accelerograms have been used for input into non-linear time-history analyses for quantifying the amount of drift sustained by the URM walls in order that the level of damage can be ascertained.

Keywords: unreinforced masonry walls, out-of-plane, two-way bending, quasi-static behaviour, seismic.

Introduction

A major experimental program involving quasi-static out-of-plane testing of unreinforced masonry walls subject to two-way bending actions and possessing a range of aspect ratios and boundary conditions were undertaken recently at the University of Adelaide forming part of the collaborative research with University of Melbourne and Swinburne University of Technology. Details of the test results have been reported in the paper by Vaculik et al. (2005) which was presented in the AEES conference at Albury. Classical hysteretic models have been calibrated to match with the behaviour recorded from the quasi-static testings. A large number of non-linear time-history analyses were then undertaken using program RUAUMOKO (Carr, 2003) based on the calibrated models. A total of 1680 floor excitations were employed to simulate the conditions of a Class C and D site and the upper levels of a six-storey building when subject to a multitude of scenarios of both near-field and far-field earthquakes. Fragility curves showing the cumulative probability of damage with increasing peak ground velocity were constructed in accordance with the proportion of cases in which pre-defined displacement limits of the wall (consistent with different damage thresholds) were exceeded by the computed displacement demands.

Hysteretic modelling

Displacement demand on URM walls can be accurately predicted by time history analyses (THA) provided that the analyses incorporate representative hysteretic models. Whilst results from a recent sensitivity study have shown that rigorous parameterisation of the hysteretic behaviour is not justified (Lumantarna et al., 2006), hysteretic modelling should feature "pinching" and strength degradation behaviour as observed from the quasi-static testing of the walls.

The "pinching" behaviour is associated with the self-centering capability of walls which is defined by the unloading part of the force-displacement relationship (refer Figure 1). Walls with perfect self-centering capability revert back to zero displacement at every instant on unloading (as represented by the origin-centered model of Figure 1a). Walls with poor self-centering capability do not recover the inelastic displacement on

unloading. The behaviour of walls at unloading can be modelled by the α parameter in the modified Takeda model (Figure 1b).

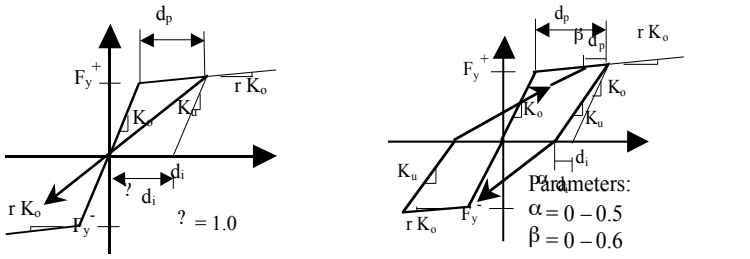

(a) Origin-Centered Model (b) Modified Takeda Model

Figure 1 Hysteretic models

Quasi-static out-of-plane loading tests were performed on eight full-scale unreinforced masonry URM wall specimens to investigate their force-displacement behaviour (Vaculik et al., 2005). The specimens consisted of two long walls without openings (4000 mm x 2500 mm), four long walls with an eccentrically positioned opening (4000 mm x 2500 mm) and two short walls with a symmetrically positioned opening (2500 mm x 2500 mm). All walls were 110 mm thick and subject to vertical pre-compression in the range 0 to 0.1 MPa. The walls were restrained from rotation along the vertical edges and laterally restrained along the top and bottom edges.

The hysteretic models shown in Figure 1 only represent the hysteretic behaviour of the two long walls without openings (walls 1 and 2) which is essentially symmetrical in terms of their "pinching" and strength degradation behaviour (Vaculik et al., 2005). Significant asymmetrical behaviour in the positive and negative displacement direction was observed from the walls with openings. The observed asymmetry has not been taken into account by the hysteretic models considered herein.

In Figures 2 and 3, the face pressure on the walls (ie. lateral loads divided by the surface area) is plotted against their deflection at mid-height. Walls with vertical pre-compression have better self-centering capability than walls without vertical pre-compression (for example, comparing Figures 1 and 2). A reasonable match between the observed hysteretic behaviour of wall 1 and the modified Takeda hysteretic model was obtained by setting the α parameter to 0.5 (Figure 2). The modified Takeda hysteretic model (with value of α parameter equal to 0.5) is shown to underestimate the self-centering capability of wall 2 (Figure 3a). The origin-centered model was used to represent the hysteretic behaviour of the wall (Figure 3b). Although the perfect self-centering capability assumption of the origin-centered model overestimates the wall self-centering capability, the origin-centered model has been shown to provide reasonable predictions of the wall maximum displacement demands (Lumantarna et al., 2006).

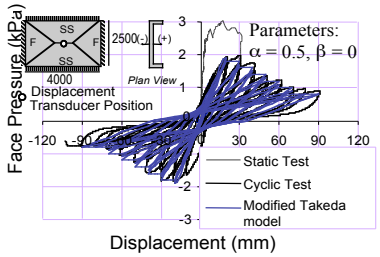

Figure 2 Hysteretic modelling of wall 1

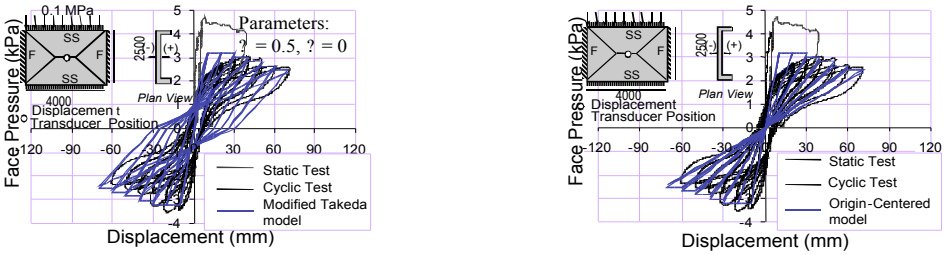

(a) Modified Takeda model (b) Origin-Centered model

Figure 3 Hysteretic modelling of wall 2

For the purposes of time-history analyses, walls can be represented as equivalent single-degree-of-freedom (SDOF) systems assuming rigid body behaviour and a fully cracked wall (Doherty et al., 2002). The effective displacement (Δe) of the equivalent SDOF systems was taken as 2/3 of the maximum displacement of the walls at mid-height. The effective mass (Me) of the wall was taken as 3/4 of its total mass. The initial behaviour of the wall in the uncracked state (ie. in the first half-cycle of the hysteresis loops which was denoted "static test" in Figures 2 and 3) has therefore been ignored. The initial periods (of a fully cracked wall) were 0.2 and 0.1 second for walls 1 and 2 respectively.

Applied excitations

Accelerograms with random phase-angles were generated by stochastic simulations of a seismological model using parameters that are considered appropriate for the attenuation conditions of southeastern Australia (Lam et al., 2000 & 2005). The simulations were based on a range of earthquake scenarios (defined by magnitude-distance combinations) which would produce peak ground velocities on rock sites ranging between 20 mm/sec and 100 mm/sec (refer Table 1). It is noted that the earthquake scenarios considered in the study included both near-field and far-field earthquakes of varying magnitude and distances.

Table 1 Earthquake scenarios with varying magnitude and distance (M-R)

PGV	20 mm/sec	40 mm/sec	60 mm/sec	80 mm/sec	100 mm/sec
M	5.5 6 6.5 7	5.5 6 6.5 7	5.5 6 6.5 7	5.5 6 6.5 7	5.5 6 6.5 7
R (km)	40 75 123 177	24 36 71 124	17 28 40 90	13 22 31 55	11 19 26 40

Accelerograms on Class C and D sites were obtained by non linear shear wave analyses of representative soil column models using program (SHAKE) and the simulated accelerograms for rock conditions as excitation input at the bedrock level (Lam et al., 2005). The shape of the simulated response spectra were generally consistent with the design response spectra stipulated by the new Australian Standard (AS/NZS 1170.4 Doc. D5212-5, 2005). Accelerograms which take into account the filtering behaviour of an unreinforced masonry six-storey building at the upper floor levels (Griffith et al., 2004) have also been obtained. These filtered excitations have been included in the analyses of URM walls to account for the filtering effects of the multi-storey buildings. In summary, a total of 1680 simulated accelerograms representing free field conditions on rock and soil sites and filtered conditions of a six-storey building have been obtained and collated.

Examples of the displacement response spectra calculated from the simulated (and filtered) accelerograms are shown in Figures 4a & 4b to reveal the significance of amplification at the natural period of the site (0.5 second and 1.0 second) and the natural period of the six-storey building (0.3 second). High spectral amplifications resulting from resonance conditions are shown at the fundamental natural period of the building (0.3 second). Exceptionally high amplification resulting from the resonance of the natural period of the building with that of a Class C site has been identified (refer Figure 4a).

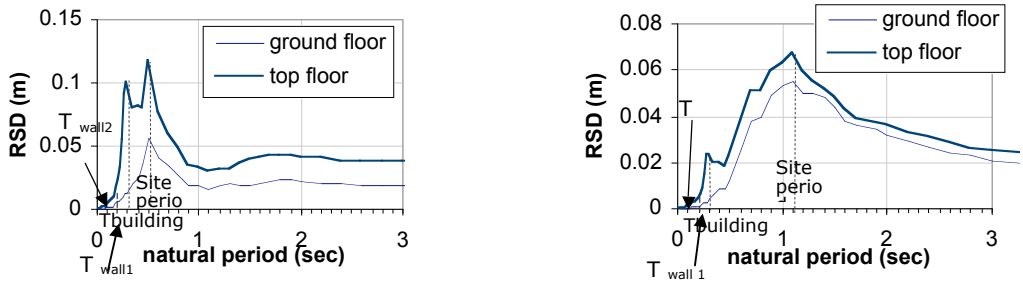

(a) Site Class C (M = 6.5, R = 40 km) (b) Site Class D (M= 6.5, R = 40 km)

Figure 4 Displacement response spectra for the top level of 6 storey building

Fragility curves of unreinforced masonry walls

The SDOF systems with hysteretic models representing URM walls were subject to non-linear time history analyses (THA) using ensembles of simulated accelerograms and computer program RUAUMOKO (Carr, 2003) to predict the wall maximum displacement demands. Load-cycle dependent strength degradation behaviour has been taken into account in the analyses.

Results from the analyses were correlated with the targeted PGV on rock sites for the construction of fragility curves based on the following limit states of damage: "minor damage", "moderate damage" and "collapse". The minor damage limit state was defined at the condition where displacement at mid-height of the wall approaches 5mm, at which the walls are expected to undergo first cracking. The displacement limit at moderate damage was arbitrarily defined at half of the wall thickness (55mm). URM walls subject to displacement exceeding this limit are expected to have a fully developed crack pattern that forms a collapse mechanism. The displacement limit at collapse was defined at the wall thickness of 110mm.

The fragility curves presented in this paper were based on force-displacement relationship of walls 1 and 2 obtained from cyclic test results. The uncertainties in the building modelling were not considered in the generation of filtered accelerograms. The random phase angle of accelerograms was assumed to be the only source of random parameters. Further fragility curves can be developed incorporating variability in material properties and dimensions of walls as well as variability in the modelling of filtering effects in building.

The statistics of the displacement demands as observed from the time-history analyses were analysed to identify the proportion of cases in which the limiting displacements of 5 mm, 55 mm and 110 mm was exceeded. Fragility curves were then constructed to correlate the cumulative probability of exceedance, $F(\nu_i)$, with increasing value of ν_i (or PGV) based on obtaining the best-fitted log-normal distribution function of equation (1) which is defined by the median and standard deviation parameters, c and β respectively.

$$F(v_i) = \Phi\left(\frac{\ln\left(\frac{v_i}{c}\right)}{\beta}\right) \qquad (1)$$

where $\Phi()$ is the cumulative log- normal distribution function

The dual parameters c and β controlling the distribution function were obtained using the well known Maximum Likelihood Method as cited by Shinozuka et al. (2001) which is briefly described in the following. The maximum likelihood parameter L is defined by equation (2).

$$L = \prod_{i=1}^{N} \left[F(v_i)\right]^{x_i} \left[1 - F(v_i)\right]^{1-x_i} \quad (2)$$

where i identifies individual analysis samples, and x_i = 1 or 0 depending on whether the limit state of damage has been exceeded, or not exceeded, in the analysis. The value of c and β was determined for the conditions where the value of L as defined by equation (2) was maximised, using equations (3a) and (3b) respectively.

$$\frac{\partial \ln(L)}{\partial c} = 0 \quad (3a) \qquad \frac{\partial \ln(L)}{\partial \beta} = 0 \quad (3b)$$

Statistical procedures as described by Shinozuka et al. (2001) have been undertaken to test the goodness of fit of the estimated fragility curves to the results from individual simulations. The analyses have shown that the values of parameters c and β estimated for the construction of fragility curves are the true values under the significance level of 10%.

An example of fragility curves for the minor and moderate damage limit state is shown in Figure 5 for wall no. 1 on a class C site incorporating filtered conditions of a multi-storey building.

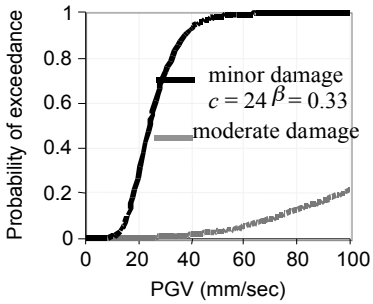

Figure 5 Fragility curves for wall 1 (subject to excitations on site class C)

The development of the fragility curve of Figure 5 had incorporated an equal number of accelerograms simulated for the earthquake scenarios considered in the study (as tabulated in Table 1). It is further shown in Table 2 that the cumulative probability of exceedance, $F(\nu_i)$, as calculated from the individual earthquake scenarios could be very different even though they were associated with a common PGV. It was implicitly assumed in the construction of the fragility curve that there were equal contributions from each of the identified earthquake scenarios for a given PGV. It should be noted that this assumption is contrary to reality as earthquake scenarios of different magnitudes could have different contributions to the potential seismic hazard of an area. The relative weighting of the scenarios cannot be generalised as it is dependent on the nature and configuration of the seismic sources affecting the area.

A de-aggregation plot such as that presented by Koo et al. (2000) in a seismic hazard modelling study for Melbourne can be used to determine the relative contributions of individual earthquake scenarios to the aggregated seismic hazard. The weighting factors inferred from that study were taken and presented in Table 3 as the C(M,R) factors. The weighted aggregated probability of exceedance was then obtained by summing the product of the $F(\nu_i)$ values of Table 2 and the C(M,R) factors of Table 3 for a given value of PGV. The "revised" fragility curve for wall 1 so obtained from this method of calculation is shown in Figure 6. The significance of the "weighting" factors can be seen by comparing Figure 5 and Figure 6a.

Table 2 Probability of exceedance for minor damage based on individual earthquake scenarios

PGV / M	20 mm/sec		40 mm/sec		60 mm/sec		80 mm/sec		100 mm/sec	
	R (km)	$F(\nu_i)$	R (km)	$F(\nu_i)$	R (km)	$F(\nu_i)$	R (km)	$F(\nu_i)$	R	$F(\nu_i)$ (km)
5.5	40	0	24	0.01	17	0.06	13	0.15	11	0.28
6	75	0.01	36	0.04	28	0.1	22	0.17	19	0.25
6.5	123	0	71	0	40	0.03	31	0.1	26	0.21
7	177	0	124	0	90	0	55	0.03	40	0.14

Table 3 Weighting factors defining the relative contributions of the individual earthquake scenarios

PGV / M	20 mm/sec		40 mm/sec		60 mm/sec		80 mm/sec		100 mm/sec	
	R (km)	C(M,R)	R (km)	C(M,R)	R (km)	C(M,R)	R (km)	C(M,R)	R (km)	C(M,R)
5.5	40	0.56	24	0.47	17	0.53	13	0.6	11	0.56
6	75	0.22	36	0.23	28	0.23	22	0.26	19	0.25
6.5	123	0.11	71	0.19	40	0.12	31	0.07	26	0.13
7	177	0.11	124	0.11	90	0.12	55	0.07	40	0.06

Fragility curves for wall no. 2 which was characterised by a pre-compression of 0.1MPa have also been constructed (Figure 7). Walls without pre-compression (wall 1) are more vulnerable to damage than walls with pre-compression (wall 2) (comparing Figures 6 with 7). Fragility curves constructed for a more onerous site class (Figures 6b and 7b) indicate less damage predicted on walls which are located on the onerous site class.

Further fragility curve has been constructed to show the significance of filtering effects of a multi-storey building (Figure 8). The fragility curve presented in Figure 8 indicates that wall 1 located at the top of a multi-storey building is most vulnerable to damage. This is attributed to the filtering effects of a multi-storey building which is of particular importance as walls without vertical pre-compression (wall 1) are typically located near the top of multi-storey buildings. However, the fragility curve shows that the wall is safe from collapsing under the filtered excitations, assuming the boundary conditions are maintained.

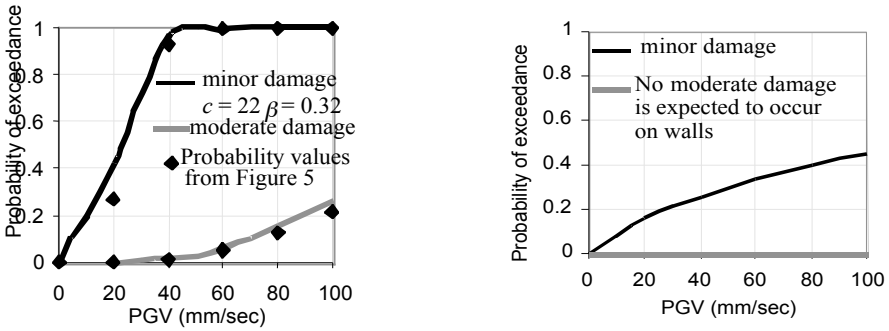

(a) subject to earthquake excitations on class site C (b) subject to earthquake excitations on class site D

Figure 6 Fragility curve for wall 1

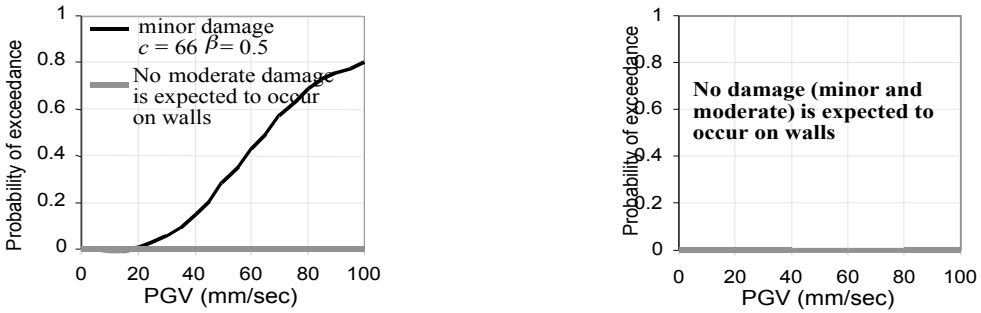

(a) subject to earthquake excitations on class site C (b) subject to earthquake excitations on class site D

Figure 7 Fragility curve for wall 2

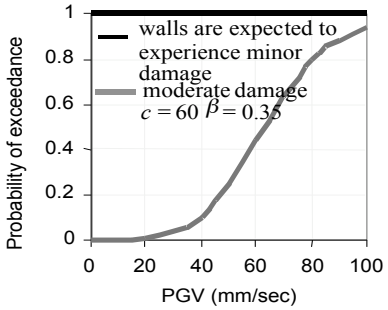

Figure 8 Fragility curve for wall 1 located at the top floor of 6-storey building on class site C

Conclusions

Fragility curves which define the probability of URM walls sustaining minor and moderate damage in an earthquake have been presented. The fragility curves were developed based on the hysteretic behaviour obtained from the quasi-static testing on URM walls. Accelerograms employed in the construction of fragility curves were generated using stochastic simulations taking into account multitude earthquake scenarios representing earthquakes of different levels of intensity, site conditions and building types. Walls without pre-compression located at the top of multi-storey buildings founded on site class C soil were shown to be most vulnerable to damage. However, none of the walls are expected to collapse under an earthquake with level of intensity associated with the seismic hazard of Australia assuming a 500 year return period and that the support conditions are maintained.

References

AS/NZS 1170.4 Draft no.D5212-5.1 (2005). Structural Design Actions – Part 4 Earthquake Actions, sub-committee BS-006-11, Standards Australia

Carr, A. J. (2003) "Ruaumoko, The Maori God of Volcanoes and Earthquakes", University of Canterbury, New Zealand

Doherty, K., Griffith, M. C., Lam, N., Wilson, J. (2002). "Displacement-based seismic analysis for out-of-plane bending of unreinforced masonry walls", Earthquake Engineering and Structural Dynamics, Vol. 31, pp. 883-850

Griffith, M., Lam, N., Wilson, J. (2004). "Displacement-based design of face-loaded masonry walls", 13thWorld Conference on Earthquake Engineering, Paper No. 2463

Koo, R., Brown, A., Lam, N., Wilson, J., Gibson, G. (2000). "A full range response spectrum model for rock sites in the Melbourne Metropolitan Area", Australian Earthquake Engineering Society Proceedings of the 2000 Conference, Paper No. 16

Lam, N., Wilson, J., Hutchinson, G. (2000). "Generation of synthetic earthquake accelerograms using seismological modelling: a review", Journal of Earthquake Engineering, Vol. 4, No. 3, pp. 321-354

Lam, N., Wilson, J., Venkatesan, S. (2005). "Accelerograms for dynamic analysis under the new Australian Standard for earthquake actions", Electronic Journal of Structural Engineering, Vol. 5, pp. 10-35

Lumantarna, E., Lam, N. T. K., Wilson, J., Griffith, M., Vaculik, J. (2006). "The out-of-plane dynamic behaviour of unreinforced masonry walls", The 19th Australasian Conference on the Mechanics of Structures and Materials, In Press

Vaculik, J., Griffith, M., Lam, N., Wilson, J., Lumantarna, E. (2005). "Cyclic response of unreinforced clay brick masonry walls", Australian Earthquake Engineering Society Proceedings of the 2005 Conference, Paper No. 40

Shinozuka, M., Feng, M. Q., Kim, H., Uzawa, T., Ueda, T. (2001) "Statistical analysis of fragility curves", Technical Report MCEER, Department of Civil and Environmental Engineering, University of Southern California, Task Numbers 106-E-7.3.5 and 106-E-7.6